Eng. Sci., 2020, 11, 85-91

Engineered Science

DOI: https://dx.doi.org/10.30919/es8a0009

Influence of the Annealing Process on Magnetic Performance of Iron Based Soft Magnetic Composites

Yan An,[1] Shuai Feng,[1] Guoqing Shao,[2] Wanli Yuan,[1] Kai Sun,[1,*] Xiaofeng Li[1] and Runhua Fan[1,*]

Abstract

In this work, the reduced iron powders were phosphated to form ferrous phosphate insulating layer on their surface. Then the iron based soft magnetic composites (SMCs) were prepared successfully by powder metallurgy and annealing process. The presence of insulating layer decreased the eddy current loss of iron powders. Furthermore, the effect of the annealing process on magnetic performance was investigated. The appropriate annealing temperature and holding time were carried out in this work. The samples were annealed in a N_2 atmosphere from 550 to 650 °C and kept for 10 to 30 min. According to the results, the phosphated iron based SMCs that were annealed in a N_2 atmosphere at 600 °C for holding 15 min of holding time had the satisfying magnetic properties. It has a high resistivity (ρ) of 0.0173 Ω·cm, a high saturated magnetic flux density (B_s) of 1.408 T, a high maximum permeability (μ_m) of 263, a low coercivity (H_c) of 197 A/m and a low core loss (P_s) of 119.70 W/kg at 1000 Hz (B_m=1 T).

Keywords: soft magnetic composites, metallurgy powders, annealing process, magnetic performance.
Received: 3 March 2020, Accepted: 6 April 2020.
Article type: Research article.

1. Introduction

The iron based soft magnetic composites (SMCs) have a potential value and broad developing prospects in the high-frequency electronic components field for their easily flexible design and low eddy current loss.[1-3] They can be pressed into desirable shapes using the powder metallurgy technology. Moreover, the insulating layer on the surface of iron powders effectively decreases the internal and external eddy current of raw iron powders.[4] Compared with conventional coating materials such as SiO_2, Al_2O_3 and epoxy resin,[5-12] the phosphated iron powders have the advantage in avoiding the external impurity during the in-situ generating ferrous phosphate process. Meantime, the thickness of ferrous phosphate insulating layer is easy to be controlled by adjusting the concentration of phosphate acid and reacting conditions. Therefore, it has a great potential value in an industrial batch production with high economic benefits.

On the other hand, it is reported that the introduced non-ferromagnetic insulating layer can lead to a magnetic dilution.[13-15] For this reason, the annealing process was applied in order to eliminate this adverse effect.[16] The aim of annealing process is to eliminate the residual stress of the iron based SMCs during the molding process and then to improve the permeability and saturated magnetic flux density.[17] In the annealing process, the annealing temperature and holding time are two important factors in order to release the residual stress of internal iron powders. Moreover, the defects and holes in the iron powders can be eliminated in the annealing process, which makes a dense internal structure of the molded SMCs and then improves the magnetic performance. Based on this fact, the effect of annealing process on the magnetic performance of iron based SMCs was investigated by adjusting the annealing temperature and holding time in this paper.

2. Experimentals

2.1. Materials

The reduced iron powders with an average particle size of 50 μm were supplied by Jingchuang Co., Ltd (China). The purity of Fe was above 99 %. The phosphoric acid, alcohol and zinc

[1]*College of Ocean Science and Engineering, Shanghai Maritime University, Shanghai, 201306, China.*
[2]*Shandong Jingchuang Magnetoelectric Industry Technology Research Institute Co., Ltd. Shandong, 276000, China.*
**E-mail: kais@shmtu.edu.cn (K. Sun); rhfan@shmtu.edu.cn (R. Fan).*

stearate were supplied by Sinopharm Chemical Reagent Co., Ltd (China).

2.2. Preparation of iron based SMCs

Firstly, the phosphoric acid was diluted by the alcohol, then the raw iron powders were added to coat the surface of iron powders by ferrous phosphate. After that, pure iron powders were separated and dried for 30 min. The zinc stearate powders (0.2 wt% of iron powders) as the lubricant were mixed with the prepared powders. Subsequently, the phosphated iron powders were cold-compacted into annular samples (40 mm outer diameter, 32 mm inner diameter and 9 mm height) under a 1000 MPa pressure. Eventually, the prepared samples were annealed in the N_2 atmosphere. In order to investigate the effect of annealing process, the annealing temperature were designed from 550 to 650 ºC and the holding time from 10 to 30 min, respectively.

2.3. Materials characterization

The microstructure analysis and phase identification for the prepared SMCs were characterized by scanning electron microscopy (SEM, FEI Quanta 650) and X-ray diffraction (XRD, Bruker D8), respectively. The mass loss after the annealing process was measured by a thermal gravimetric analyzer (HS, TGA-101). The resistivity was measured by a four-point probe resistance analyzer (Kunde, KDY-1) at room temperature. The magnetic properties, including saturated magnetic flux density (B_s), maximum permeability (μ_m), core loss (P_s) and coercivity (H_c) were measured by a silicon steel material testing device (Lianzhong, Co., Ltd., MATS-3000M). The measurement frequency was below 1000 Hz.

3. Results and discussion

Fig.1 shows the SEM images of the raw iron powders (Fig.1a) and phosphated iron powders (Fig.1b). It can be seen that pure iron powders had a rough and irregular surface, as shown in Fig.1a. After processed by the phosphate acid, the surfaces of iron powders were coated by a uniform and smooth insulating layer (Fig. 1b). The composition and elements analysis are shown in Fig. 1c. The iron, phosphate and oxide elements were detected on the surface of phosphated iron powders by the mapping scan. According to the acquired table of the element contents, the mass fraction (wt%) of P element was 7.45. However, the wt% of P element in ferrous phosphate was 18.9. This result indicates that the surface of iron powders is not completely covered by the ferrous phosphate.

The compositions of raw powders and phosphated iron powders with different annealing temperatures (from 550 to 650 ºC) were detected by the X-ray diffraction measurement, as shown in Fig. 2. It can be seen that the characteristic peaks (110), (200), (211) and (220) of the Fe phase were observed. Moreover, the intensity of the peaks from the Fe phase became stronger with the increase of the annealing temperature, which resulted from the improved recrystallization degree of iron powders in the annealing process. The peaks from ferrous phosphate compounds on the surface of iron powders were not distinctly observed. The reason is that the phosphate compounds exist in the form of amorphous. Meanwhile, the amorphous ferrous phosphate insulating layer could be too thin to be detected by the X-ray.

The FT-IR spectra of the iron based SMCs are depicted in Fig. 3. The chemical bond of PO_4^{3-} from the ferrous phosphate can be verified by the presence of characteristic peaks, which appear at around 570 and 1040 cm^{-1}, respectively. The characteristic peak at around 3400, 1630 and 1380 cm^{-1} represent the vibration absorption peak of -OH. The vibration peaks at 2850 and 2924 cm^{-1} correspond to the $-CH_2$ and $-CH_3$. The peak at around 2360 cm^{-1} can be attributed to the asymmetric stretching vibration of -NH, which originates from the impurities in the iron powders. According to the FT-IR spectra, it can be judged that ferrous phosphate was formed on the surface of iron powders.

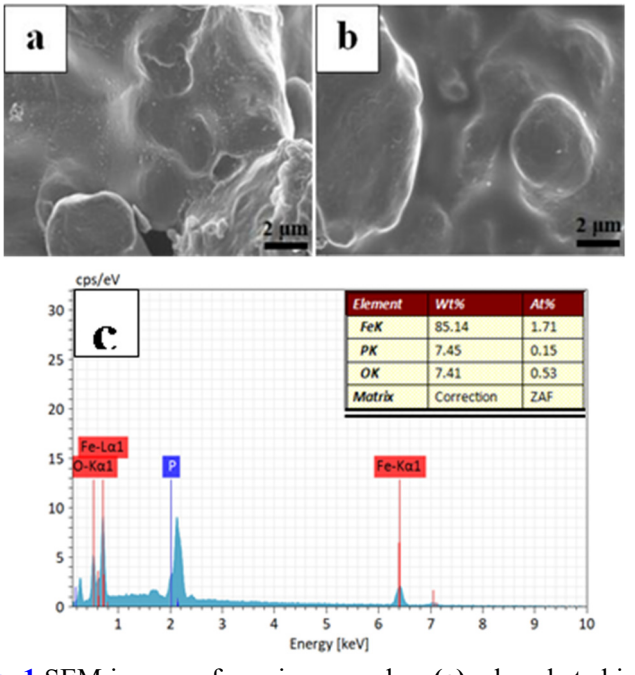

Fig. 1 SEM images of raw iron powders **(a)**, phosphated iron powders **(b)**, and elemental analysis **(c)**.

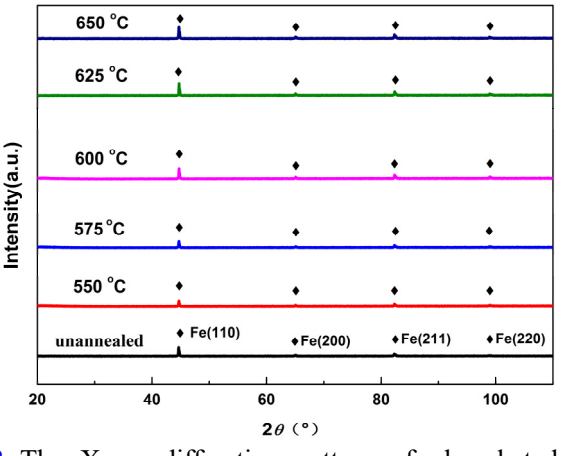

Fig. 2 The X-ray diffraction pattern of phosphated iron powders with different annealing temperatures.

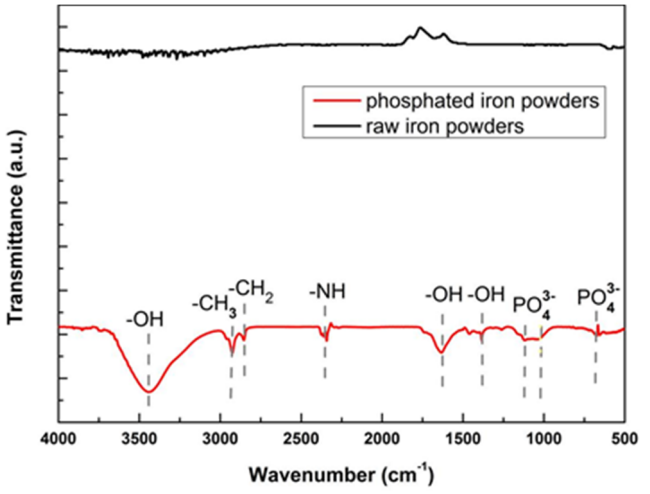

Fig. 3 The FT-IR spectra of raw iron powders and phosphated iron powders.

Fig. 4 shows the thermal gravimetric analysis (TGA) curve of the iron based SMCs. For this measurement process, it is different from conventional measurement that the heating rate is variable to match the actual annealing process. The first weight mass can be observed at around 180 °C, which originates from the evaporation of crystal water. The process can be described as follows:

$$Fe_3(PO_4)_2.8H_2O \xrightarrow{180\ ^oC} Fe_3(PO_4)_2 + 8H_2O \qquad (1)$$

It results from the weight loss of crystal water in the ferrous phosphate. Besides, it can be seen that the mass loss is about 0.3 % when the temperature reaches 280 °C, which corresponds to the evaporation of zinc stearate and the lubricant. The weight mass at 370 °C corresponds to the oxidation process of ferrous phosphate. When the temperature attaches at around 485 °C, it has a small weight loss. According to the previous investigation,[18-19] the ferrous phosphate that was coated on the surface of iron powders begins to decompose at 475 °C. Thus, it can be considered that the mass loss originates from the decomposition of iron phosphate insulting layer.

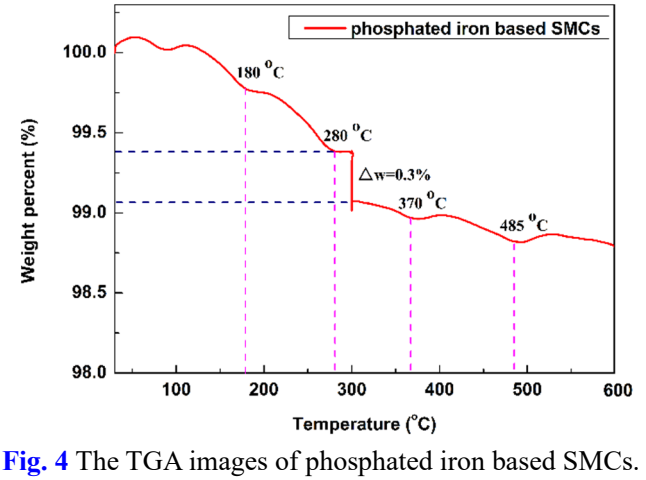

Fig. 4 The TGA images of phosphated iron based SMCs.

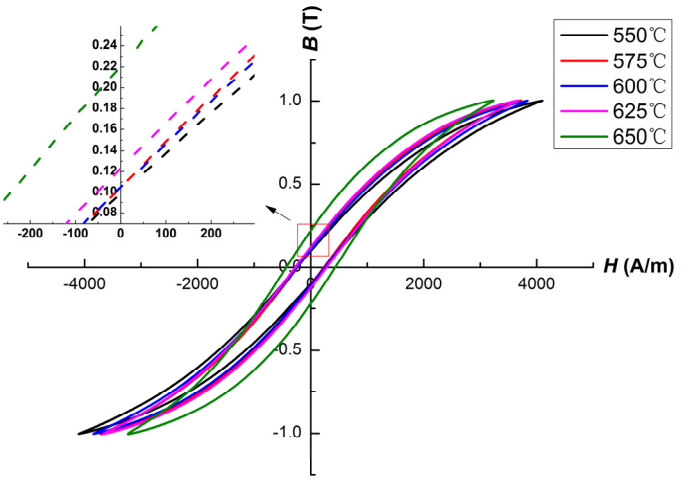

Fig. 5 The static hysteresis loops of the prepared phosphated iron based SMCs; the inset shows the enlarged part of the hysteresis loops.

Fig. 5 shows the static hysteresis loop and residual magnetic induction (shown in the enlarged zone) of the prepared phosphated SMCs with different annealing temperatures from 550 to 650 °C. In Fig.5, it can be observed that all lines show a typical soft magnetic character with a long and narrow surrounded area. Generally, the area presents the value of hysteresis loss. The magnetic induction (B) had not reached the saturated degree when the magnetic field strength (H) was attached at 4000 A/m. With the increase of annealing temperature, the SMCs samples were easier to be magnetized because a higher temperature makes a lower internal stress and then it is convenient to the motion of domain wall. As a result, the sample annealed at 650 °C has the highest magnetic induction and residual magnetic induction (inset of Fig. 5).

The magnetic performance including maximum permeability (μ_m), saturated magnetic induction (B_s) and coercive force (H_c) are shown in Fig. 6. It suggested that the permeability and saturated magnetic induction increased when the annealing temperature changed from 550 to 650 °C.

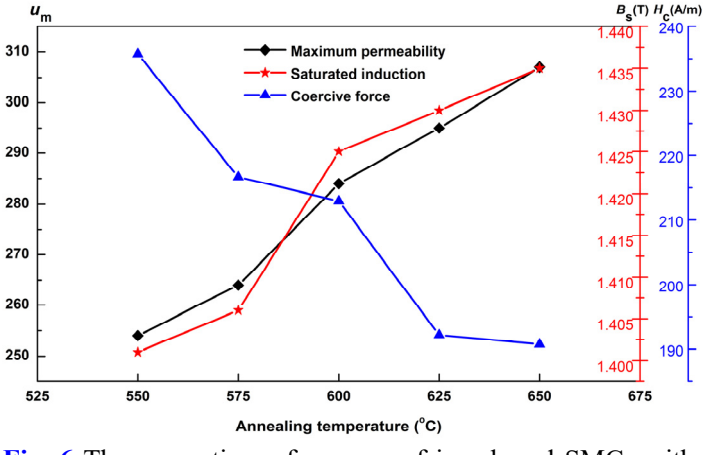

Fig. 6 The magnetic performance of iron based SMCs with different annealing temperatures.

This can be illustrated by the following reason. Mainly, the invalidation of the ferrous phosphate insulating layer at higher temperatures resulted in a lower non-magnetic content. Besides, according to the magnetic chip theory,[20] a higher temperature is conducive to relieving the internal stress of molding iron powders and to acquiring a better crystal structure. For the same reason, the coercive force dropped with the increase of annealing temperature.

In Table 1, the density, resistivity and core loss of phosphated SMCs with different annealing temperatures from 550 to 650 °C are listed. It can be seen that the density of SMCs hardly changed with increasing the annealing temperature. Moreover, as shown in Table 1, the resistivity and core loss of phosphated iron based SMCs with different annealing temperatures from 550 to 650 °C are listed. It can be obviously seen that the resistivity dropped sharply when the temperature increased from 550 to 575 °C. It confirmed that the ferrous phosphate insulating layer began invalid at this temperature. Furthermore, the sample had the lowest core loss (P_s), i.e., 113.50 W/kg at 575 °C. The reason is that parts of insulating layers still existed. This conclusion can also be verified by the magnetic performance in Fig. 7. The saturated magnetic induction had a rapid rise when the annealing temperature increased from 575 to 600 °C. Combining with the data of resistivity, it can be suggested that the phosphated insulating layer got into valid totally when the annealing temperature was higher than 600 °C.

According to the above data and investigation, the prepared SMCs annealed at 600 °C had a satisfying loss and a better magnetic performance. Thus, the annealing temperature was set at 600 °C to investigate the influence of holding time on magnetic performance. Fig.7 shows the magnetic performance of the samples processed at 600 °C with different annealing holding time from 10 to 30 min. The tendency of maximum permeability, saturated magnetic induction and coercive force are different from those on the condition of increasing the annealed temperature (as shown in Fig. 6), which changed in a linear manner. It is clear that the maximum value of maximum permeability, 286, saturated magnetic induction, 1.428 T and coercive force, 213 A/m appeared when the annealing time attached at 20 min. Moreover, the saturated magnetic induction was below 1.41 T when the holding time was maintained at 15 and 25 min. The reason for this non-linear variety can be suggested that the ferrous phosphate insulating layer was completely destroyed during the annealing process when the holding time was over than 15 min.

In Table 2, the density, resistivity and core loss (P_s) of phosphated SMCs with different annealing time from 10 to 30 min at 600 °C were listed. It shows that the density increases with the extension of holding time in the annealing process. The reason is that the internal stress can be released more and more fully with increasing the holding time at a certain temperature.[21] Furthermore, the internal defects and holes are also diminished.

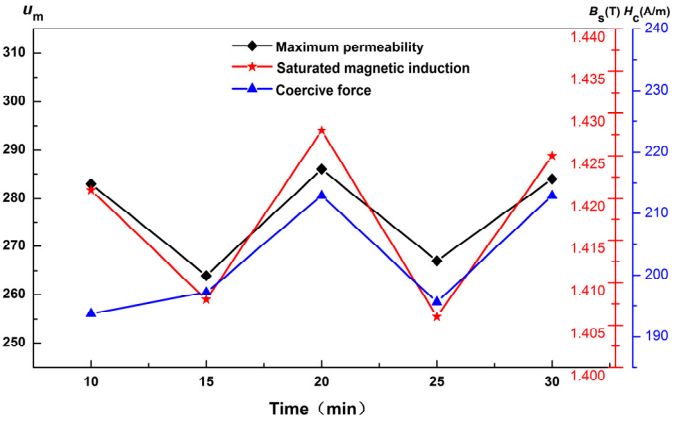

Fig. 7 The magnetic performance of iron based SMCs in 600 °C with different holding time.

Furthermore, the internal defects and holes are also diminished. Compared with the data from Table 1, it can be easily seen that the density of iron based SMCs dropped obviously from 7.46 to 7.43 g/cm^3 with the decrease of annealing time, which confirmed that the internal stress can be reduced during the annealing process. Furthermore, when the holding time attached at 15 min in 600 °C, the core loss (P_s) was reduced to the lowest value of 119.70 W/kg. As mentioned above, when the annealing time was over than 575 °C, the insulating layer has been destructed totally. At this condition, the extended holding time in the annealing process has no influence on the structure of iron powders. Therefore, the resistivity shows a nonlinear variation with increasing the holding time. Consequently, the P_s was mainly affected by the hysteresis loss.

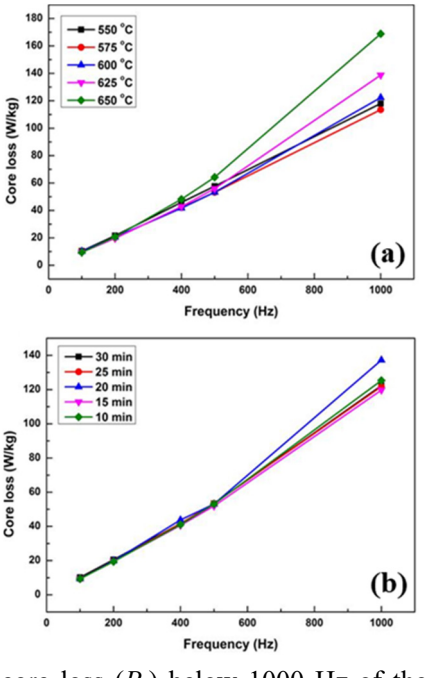

Fig. 8 The core loss (P_s) below 1000 Hz of the iron based SMCs with **(a)** different annealing temperatures and **(b)** holding time.

Table 1. The resistivity and core loss (P_s) for the prepared SMCs with different annealing temperatures.

Annealing temperature (°C)	Density (g/cm^3)	Resistivity (Ω·cm)	***Ps* @ *Bm* = 1 T (W/kg)** Frequency (Hz)				
			100	200	400	500	1000
550	7.46	40.0741	10.44	21.62	45.88	57.68	118.00
575	7.47	0.2004	9.93	20.23	42.08	53.21	113.50
600	7.46	0.0908	10.20	20.53	41.70	53.29	122.33
625	7.47	0.0099	9.48	19.66	42.85	55.88	138.73
650	7.47	0.0042	9.44	20.69	48.19	64.19	168.83

Fig. 8 directly shows the core losses with different annealing temperatures and holding time for the prepared iron based SMCs. The measurement frequency points are 100, 200, 400, 500 and 1000 Hz, respectively. As shown in Fig. 8a, the P_s grew slowly with the increase of frequency from 100 to 400 Hz, then had a rapid growth when the frequency was over than 600 Hz. It has the same trend for the P_s with different holding time, as shown in Fig. 8b. For the iron based SMC, the P_s is usually composed of hysteresis loss (P_h), eddy current loss (P_e) and residual loss (P_r). Usually, the P_r can be ignored at a low frequency. Thus, the total core loss for the SMCs can be expressed by Equations (2) and (3):[22]

$$P_s = P_h + P_e + P_r \quad (2)$$

$$P_h = C_h B_m^n f \quad (3)$$

where the C_h represents the coefficient for hysteresis loss, B_m represents the maximum magnetic flux density and f is the test frequency. In this work, the B_m was a fixed value in the measurement process. According to the previous investigation,[23] the P_e can be classified into two parts: the inter eddy current loss (P_e^{in}) and intra eddy current loss (P_e^{tra}) of particles, which can be described by the following formula:[24]

$$P_e^{in} = C_e^{in} B_m^2 f^2 = \pi^2 d_{eff}^2 B_m^2 f^2 / \rho_s \beta_1 \quad (4)$$

$$P_e^{tra} = C_e^{tra} B_m^2 f^2 = \pi^2 d^2 B_m^2 f^2 / \rho_p \beta_2 \quad (5)$$

In this formula, d is related to the size of iron particle and d_{eff} is related to the effective size, which means the average size of integral iron powders; β_1 represents the rectangular geometrical factor and β_2 represents the granular geometrical factor, which depends on the geometry of iron particle; ρ_s and ρ_p can be regarded as the bulk resistivity of molded samples and intra-particle resistivity of iron powders.[25,26]

For the prepared phosphated iron based SMCs, raw materials and the molding process were controlled in the same condition, so the d, d_{eff}, β_1 and β_2 had nearly the same values. Based on this fact, the core loss was determined by the C_h, C_e^{ter} and C_e^{tra} at the same frequency. The C_h represents the coefficient for the hysteresis loss and the C_e^{ter}, C_e^{tra} represent the coefficients for the eddy current losses, which are related to the changes of external magnetic field and the size, resistivity of measured samples. At this condition, the value of core loss only depends on the annealing process. Appropriate temperature and holding time can release enough internal stress inside the iron powders and keep the ferrous phosphate insulating layer from being damaged. Under this condition, the iron based SMCs had lower values of C_h, C_e^{ter}, C_e^{tra} and higher values of ρ_s and ρ_p.

Table 2. The resistivity and core loss (P_s) for prepared SMCs with different annealing time at 600 °C.

Annealing time (min)	Density (g/cm^3)	Resistivity (Ω·cm)	***Ps* @ *Bm* = 1 T (W/kg)** at frequency (Hz)				
			100	200	400	500	1000
30	7.46	0.0908	10.20	20.53	41.70	53.29	122.33
25	7.45	0.0159	9.28	19.57	41.65	53.35	121.77
20	7.45	0.0131	9.38	19.83	43.75	53.01	137.23
15	7.44	0.0173	9.50	19.53	40.63	51.89	119.70
10	7.43	0.0165	9.40	19.41	41.04	53.04	125.33

4. Conclusion

In this work, the phosphated iron based SMCs were produced by the powder metallurgy technology. Then the annealing process was applied to improve the magnetic performance simultaneously. In order to acquire both high permeability, saturated magnetic induction and low core loss, the effects of annealing temperature and holding time on the magnetic performance of the SMCs were investigated. According to the results, the phosphated iron based SMCs which were annealed in a N_2 atmosphere at 600 °C for 15 min had the satisfying magnetic properties. It has a high resistivity (ρ) of 0.0173 Ω·cm, a high saturation magnetic flux density (B_s) of 1.408 T, a high maximum permeability (μ_m) of 263, a low coercivity (H_c) of 197 A/m and a low core loss (P_s) of 119.70 W/kg at 1000 Hz (B_m=1 T). This work provides a promising annealing route to produce iron based SMCs with excellent magnetic performances and low core losses.

Acknowledgements

The authors gratefully acknowledge the financial supports by the National Natural Science Foundation of China (Grant No. 51803119, 51871146 and 51771108), the Innovation Program of Shanghai Municipal Education Commission (Grant No. 2019-01-07-00-10-E00053), Chenguang Program supported by Shanghai Education Development Foundation and Shanghai Municipal Education Commission (Grant No. 18CG56) and the Science and Technology Commission of Shanghai Municipality (Grant No. 18DZ1112900) and Shanghai Engineering Technology Research Centre of Deep Offshore Material (19DZ2253100).

Conflict of Interest

There is no conflict of interest.

Supporting Information

Not Applicable.

References

[1] A. H. Taghvaei, H. Shokrollahi and K. Janghorban, *J. Magn. Magn. Mater.*, 2009, **321**, 3926-3932, doi: 10.1016/j.jmmm.2009.07.061.
[2] S. Wu, A. Sun, Z. Lu and C. Cheng, *Mater. Chem. Phys.*, 2015, **153**, 359-364, doi: 10.1016/j.matchemphys.2015.01.026.
[3] M. Strečková, Ľ. Medvecký, J. Füzer, P. Kollár, R. Bureš and M. Fáberová, *Mater. Lett.*, 2013, **101**, 37-40, doi: 10.1016/j.matlet.2013.03.067.
[4] B. Yang, Z. Wu, Z. Zou and R. Yu, *J. Phys. D-Appl. Phys.*, 2010, **43(36)**, 365003, doi: 10.1088/0022-3727/43/36/365003.
[5] S. Wu, A. Sun, W. Xu, Q. Zhang, F. Zhai, P. Logan and A. A. Volinsky, *J. Magn. Magn. Mater.*, 2012, **324**, 3899-3905, doi: 10.1016/j.jmmm.2012.06.042.
[6] A. H. Taghvaei, H. Shokrollahi, K. Janghorban and H. Abiri, *Mater. Design*, 2009, **30**, 3989-3995, doi: 10.1016/j.matdes.2009.05.026.
[7] S. Wu, J. Fan, J. Liu, H. Gao, D. Zhang and A. Sun, *J. Supercond. Nov. Magn.*, 2018, **31**, 587-595, doi: 10.1007/s10948-017-4256-5.
[8] P. Xie, K. Sun, Z. Wang, Y. Liu, R. Fan, Z. Zhang and G. Schumacher, *J. Alloy. Compd.*, 2017, **725**, 1259-1263, doi: 10.1016/j.jallcom.2017.04.248.
[9] P. Xie, Z. Zhang, Z. Wang, K. Sun and R. Fan, *Research*, 2019, **2019**, 1021368, doi: 10.34133/2019/1021368.
[10] K. Sun, S. Feng, Q. Jiang, X. Li, Y. Li, R. Fan, Y. An and J. Wang, *J. Magn. Magn. Mater.*, 2020, **493**, 165705, doi: 10.1016/j.jmmm.2019.165705.
[11] X. Zhu, J. Yang, D. Dastan, H. Garmestani, R. Fan and Z. Shi, *Compos. Part A-Appl. S.*, 2019, **125**, 105521, doi: 10.1016/j.compositesa.2019.105521.
[12] P. Xie, Y. Li, Q. Hou, K. Sui, C. Liu, X, Fu, J. Zhang, V. Murugadoss, J. Fan, Y. Wang, R. Fan and Z. Guo, *J. Mater. Chem. C*, 2020, **8**, 3029-3039, doi: 10.1039/c9tc06378a.
[13] W. Li, W. Huang, Y. Kang, Y. Guo, Y. Ying, J. Yu, J. Zheng, L. Qiao and S. Che, *Compos. Sci. Technol.*, 2019, **173**, 7-14, doi: 10.1016/j.compscitech.2019.01.022.
[14] Y. Kang, W. Li, T. Ma, X. Huang, Y. Mo, Z. Chu, Z. Zhang and G. Feng, *Compos. Sci. Technol.*, 2019, **174**, 184-193, doi: 10.1016/j.compscitech.2019.02.029.
[15] W. Li, Z. Wang, Y. Ying, J. Yu, J. Zheng, L. Qiao and S. Che, *Ceram. Int.*, 2019, **45**, 3864-3870, doi: 10.1016/j.ceramint.2018.11.058.
[16] J. Lei, J. Zheng, H. Zheng, L. Qiao, Y. Ying, W. Cai, W. Li, J. Yu, M. Lin and S. Che, *J. Magn. Magn. Mater.,* 2019, **472**, 7-13, doi: 10.1016/j.jmmm.2018.09.125.
[17] Y. Liang, F. Ye, J. Lin, Y. Wang, G. Chen, *J. Alloy. Compd.*, 2010, **491**, 268-270, doi: 10.1016/j.jallcom.2009.10.118.
[18] G. Zhao, S. Wu and M. Yan, *J. Alloy. Compd.*, 2016, **685**, 231-236, doi: 10.1016/j.jallcom.2016.05.277.
[19] M. Huang, C. Wu, Y. Jiang and M. Yan, *J. Alloy. Compd.*, 2015, **644**, 124-130, doi: 10.1016/j.jallcom.2015.04.201.
[20] B. M. Tanygin, *J. Magn. Magn. Mater.*, 2011, **323**, 616-619, doi: 10.1016/j.jmmm.2010.10.028.
[21] S. Wu, A. Sun, F. Zhai, J. Wang, Q. Zhang, W. Xu, P. Logan and A. A. Volinsky, *J. Magn. Magn. Mater.*, 2012, **324**, 818-822, doi: 10.1016/j.jmmm.2011.09.026.
[22] O. de la Barrie`re, C. Appino, F. Fiorillo, C. Ragusa, H. B. Ahmed, M. Gabsi, F. Mazaleyrat and M. Lobue, *J. Appl. Phys.*, 2011, **109**, 07A317, doi: 10.1063/1.3554207.
[23] J. Li, J. Yu, W. Li, S. Che, J. Zheng, L. Qiao and Y. Ying, *J. Magn. Magn. Mater.*, 2018, **454**, 103-109, doi: 10.1016/j.jmmm.2018.01.061.
[24] A. H. Taghvaei, H. Shokrollahi and K. Janghorban, *Mater. Des.*, 2010, **31**, 142-148, doi: 10.1016/j.matdes.2009.06.044.
[25] W. Li, W. Wang, J. Lv, Y. Ying, J. Yu, J. Zheng, L. Qiao and S. Che, *J. Magn. Magn. Mater.*, 2018, **456**, 333-340, doi: 10.1016/j.jmmm.2018.02.033.
[26] W. Cai, H. Cai, Y. Kang, Y. Ying, J. Yu, J. Zheng, L. Qiao, Y. Jiang and S. Che, *Acta Mater.*, 2019, **167**, 267-274, doi: 10.1016/j.actamat.2019.01.035.

Publisher's Note

Engineered Science Publisher remains neutral with regard to jurisdictional claims in published maps and institutional affiliations.